Elsevier Editorial System(tm) for Journal of Materials Processing Technology

Manuscript Draft

Manuscript Number: PROTEC-D-16-00677R1

Title: Modelling of Austenite Formation during Heating in Boron Steel Hot Stamping Processes

Article Type: Research Paper

Keywords: Austenite formation; Boron steel; Constitutive modelling; Hot stamping; Phase transformation; Heating rate.

Corresponding Author: Dr. Daniel Balint, PhD

Corresponding Author's Institution: Imperial College London

First Author: Nan Li, PhD

Order of Authors: Nan Li, PhD; Jianguo Lin, PhD, Professor; Daniel Balint, PhD; Trevor A Dean, PhD, Professor

Abstract: A physically-based material model has been developed to describe the austenite formation in a manganese-boron steel during heating in hot stamping processes. The equations were formulated based on three austenite formation mechanisms: nucleation, growth and impingement. It is able to characterise the phase transformation process under both non-isothermal and isothermal conditions, where the effects of heating rate and soaking temperature on the austenite formation have been rationalised. Heat treatment tests of the manganese-boron steel were performed on a Gleeble 3800 subjected to various heating conditions (heating rate: 1 K/s - 25 K/s, soaking temperature: 1023 K - 1273 K). The dimensional changes of specimens associated with the phase transformation, which was measured using a high resolution dilatometer, has been quantitatively related to the volume fraction of austenite formation. The experimental data was used to calibrate and validate the equations. Good agreement between the experimental and predicted results has been obtained. Further analysis has been made to illustrate the significance of the model in applications.

Imperial College
London

Department of Mechanical Engineering
Imperial College London
London SW7 2AZ
Tel: +44 (0) 207 594 7084
Fax: +44 (0) 207 594 7010

d.balint@imperial.ac.uk
www.imperial.ac.uk/people/d.balint

23 May 2016

Dr Daniel S Balint PhD
Reader in Solid Mechanics

Dear Professor Allwood,

Modelling of Austenite Formation during Heating in Boron Steel Hot Stamping Processes
N. Li, J. Lin, D. S. Balint,*, T. A. Dean

Thank you for the reviewers' comments on our paper, which are very valuable to us and helped us to improve the manuscript.

The manuscript has been modified according to the reviewers' comments. Our replies to the reviewers and can be found in the document 'Li et al Responses'.

I should be grateful if you would consider this revised version of our original paper for publication in Journal of Materials Processing Technology. The paper is not being submitted for publication elsewhere.

Sincerely,

Daniel Balint

PROTEC-D-16-00677

Response to Reviewers' Comments

We sincerely thank the reviewers' for their detailed feedback on our manuscript. We have addressed all comments to the best of our abilities, and feel the manuscript is now improved as a result. All modifications to the manuscript have been highlighted in the revised manuscript document. We hope the revised manuscript is now suitable for publication in Journal of Materials Processing Technology.

Reviewer #1: The paper is very well presented and clearly written with a good selection of relevant references. The model developed follows the established theories for nucleation and growth with a useful modification to cope with holding in the intercritical range. The results appear to give a good prediction of the industrial process of hot stamping and therefore the paper is highly relevant to the subject matter of the journal.

There are a few minor areas that could be changed to improve the quality of the paper as follows:-

1. The composition in Table 1 is a maximum value as published by the steel manufacturer for this grade and may be significantly different to the actual steel used in these investigations. Ideally the actual composition of the heat that was used should be reported. If this is not possible then a minimum should also be added to the table to show the potential range in composition that the actual experimental steel could lie within.

Thanks for this comment.
The chemical composition from the material mill certificate has only max values, which was provided by the company. While we appreciate the reviewer's comment on this and agree it would be nice to include minimum values to show the range, we are simply unable to provide further information for this commercial alloy. We have faithfully reported the information that is available on composition of this commercial alloy.

---

2. A critical re-evaluation of P.10 is needed with respect to nucleation sites in the light of this steel being 0.22%C and the absence of any experimental evidence being supplied for this steel to back up the assertions regarding nucleation sites. The impression is given that nucleation only takes place within pearlite - supported by citing papers related to eutectoid steels (this steel has around 20-30% pearlite only). While nucleation will occur in pearlite, early studies of the transformation of ferrite / pearlite microstructures to austenite state that nucleation occurs preferentially at

pearlite / pearlite boundaries, ferrite / pearlite boundaries (also see section 2.1.2.2 of Savran's Thesis) or at grain boundary carbides on ferrite-ferrite boundaries(e.g. Carpenter & Robertson, JISI, 127, No.1, 1933 (p.259).
The assumption that no nucleation can take place at ferrite grain boundaries as implied by equations (4) needs justification or at least comment on the effect that this assumption has on potential accuracy of the model. One would assume that at very high heating rates nucleation could occur at ferrite grain boundaries. In fact chapter 5 of Savran's Thesis shows continuous nucleation for a 0.22%C steel (25% of nuclei formed at higher temperatures) which is very similar in C content to the hot stamping grade considered in this paper. The expected site saturation does occur in 0.35%C steels according to her work.

Many thanks for this comment. More explanation has been added on P.10 to address this issue - mainly based on research from Savran's Thesis (the discussion in chapter 4). The observation of nuclei in pro-eutectoid ferrite regions in C22, as mentioned, was because the material was heated up at a slow heating rate – 10 °C /min (as given in chapter 3 of the thesis). For the steel examined in this study for hot stamping applications, the heating rate is much higher. This is discussed in the amendments to the manuscript on P.10.

---

3. Section 3.3
"Only partial austenite formation cannot be achieved" (I think this should read "can be achieved / is achieved"?)

Thank you. You are right! That was a typo and has been corrected.

Reviewer #2: A nice piece of modeling and good materials science of practical meaning.

Thank you very much!

Modelling of Austenite Formation during Heating in Boron Steel Hot Stamping Processes

N. Li[a], J. Lin[a], D. S. Balint[a,*], T.A. Dean[b]

[a] Department of Mechanical Engineering, Imperial College London, London, SW7 2AZ, UK

[b] School of Mechanical Engineering, The University of Birmingham, Birmingham B15 2TT, UK

Abstract

A physically-based material model has been developed to describe the austenite formation in a manganese-boron steel during heating in hot stamping processes. The equations were formulated based on three austenite formation mechanisms: nucleation, growth and impingement. It is able to characterise the phase transformation process under both non-isothermal and isothermal conditions, where the effects of heating rate and soaking temperature on the austenite formation have been rationalised. Heat treatment tests of the manganese-boron steel were performed on a Gleeble 3800 subjected to various heating conditions (heating rate: 1 K/s – 25 K/s, soaking temperature: 1023 K – 1273 K). The dimensional changes of specimens associated with the phase transformation, which was measured using a high resolution dilatometer, has been quantitatively related to the volume fraction of austenite formation. The experimental data was used to calibrate and validate the equations. Good agreement between the experimental and predicted results has been obtained. Further analysis has been made to illustrate the significance of the model in applications.

Keywords: Austenite formation; Boron steel; Constitutive modelling; Hot stamping; Phase transformation; Heating rate.

*Corresponding author. Email: d.balint@imperial.ac.uk. Tel.: +44 (0) 207 594 7084.

1. Introduction

The rising demand for increasing safety and reducing weight of car bodies in the automotive industry has stimulated technological innovation in sheet metal forming. Hot stamping of boron steel for safety critical parts has therefore been well developed. Conventionally, as summarised by Karbasian and Tekkaya (2010), during the process blanks are firstly austenitized, and subsequently formed and quenched in cold dies, so that ultra-high strength parts in the martensite phase are obtained. Now, a novel strategy about selective heating and press hardening of boron steels has been proposed by the authors (Li et al., 2012; Li et al., 2014) to produce parts with a tailored distribution of mechanical properties, which introduces the potential for making parts that conform to functional requirements. In this process, a blank is heated under tailored thermal conditions, which enables part of the steel to be fully or partially austenitized while the other part experiences no phase transformation. Thus, after hot stamping and cold die quenching, the fraction and distribution of martensite in the as-formed part is determined by the extent of austenitization, which means that control of austenitization during the heating process is of primary importance in deciding the final properties for a given part. Therefore, understanding and modelling the relationship between heating conditions and the formation of austenite is paramount to optimizing the thermal cycle for innovative hot stamping processes.

Studies on austenite formation, compared with the number of investigations into the decomposition of austenite during cooling, have been few and incoherent until the 1980's, as stated by Law and Edmonds (1980). Then, as reported by Garcia and Deardo (1981), driven by automotive applications, great interest in the heating stage of thermal cycles was stirred by the development of advanced high strength steels (AHSS). Attention was drawn from full

austenitization to partial austenitization in intercritical annealing practices, since it offers a means of optimizing the mechanical properties of dual-phase steels. A classic study on the kinetics of austenite formation in dual-phase steels containing different percent of carbon during intercritical annealing was conducted by G. R. Speich (1981). Since then, more extensive and systematic research on the austenite formation has been carried out to gain quantitative understanding of microstructural evolution during the transformation and the mechanisms that control it under different conditions. For example, Asadi Asadabad et al. (2008) characterised the relationship between temperature and time of intercritical annealing and transformed fraction of austenite in dual phase steels; Oliveira et al. (2007) investigated the effects of heating rates on critical temperatures of austenite formation in a low carbon steel. However, information on austenitization in boron steels for hot stamping application is still sparse. Cai (2011) focused only on full austenitization under continuous heating-up without considering isothermal annealing. The effects of heating rate and temperature on the full/partial transformation of austenite in boron steels, under both non-isothermal and isothermal conditions, were characterised for the first time by the authors (Li et al., 2016).

Various austenitization models have been developed in recent years. According to (Savran, 2009), these can generally be classified as probabilistic models and deterministic models. The former type introduces the stochastic variables into calculation process, which can account for the stochastic character of the phase transformation and give qualitative representation of the microstructure, e.g. Haddad-Sabzevar et al. (2009) employed a stochastic model to simulate the austenite phase formation and its growth during welding of a low alloy steel and to visualize the topology of the austenite phase. The latter type is based on the time-integration of equations consisting of certain state variables, so as to characterize the microstructural evolution, at various length scales, depending on the features of interest,

throughout the phase transformation. As reported by Azizi-Alizamini (2010), deterministic models for describing the austenite formation are predominant in the literature, developed using analytical and phenomenological approaches Analytical approaches are mainly based on the analysis of mechanisms which control the austenite front migration, which requires assumptions (e.g. on growth modes) that are strictly defined in advance. However, this may not be easy when the phase transformation mode is of a complex character, which was pointed out by Parris and McLellan (1976). According to the investigation by Schmidt et al. (2007)), for austenitization in a manganese-boron steel with a ferrite-pearlite starting microstructure, depending on heating conditions, the growth of the austenite phase can be controlled by interface reaction or volume diffusion, and the latter could be carbon diffusion in austenite or manganese diffusion in ferrite. In this case, an analytical approach may not be efficient. Phenomenological approaches are mainly conducted by relating the transformation progress to the change of austenite volume fraction with time. Chen et al. (2010) reported that Avrami's equation plays a critical role in the fundamental understanding of the transformation but it is too simple to adapt to any specific case, e.g. a transformation that has mixed nucleation or an alternate growth mode. Hence extensive studies have been conducted to further develop this equation, so as to fit it to different transformation conditions.

However, the transformations of austenite under isothermal and non-isothermal conditions have always been modelled separately. Thus the effects of heating rate on the subsequent isothermal transformation cannot be accounted for. In hot stamping, the boron steel is treated with continuous heating followed by steady soaking; in addition, intercritical annealing for partial austenitization is involved under selective heating conditions. Therefore, an austenite formation model which can be applied to this complex heating condition is needed.

The main aim of this work was to develop a set of equations that can effectively describe the austenite formation in boron steel, under both non-isothermal and isothermal conditions within or above intercritical temperatures, for hot stamping processes. The development of the model is based on theoretical analysis of the nucleation, growth and impingement mechanisms for austenite formation. Phenomenological approaches are adopted to characterize the effects of heating conditions on the transformation. Experimental data on boron steel subjected to different heating rates and temperatures was used to determine and calibrate the model.

2. Mechanisms of austenite formation in hypoeutectoid steels

For the study of the constitution and structure of steels, stated by Azizi-Alizamini (2010), the Fe-C equilibrium diagram is the most widely-used way to represent the existence of different phases in equilibrium depending on carbon content and temperature. As shown in Figure 1(a), the equilibrium conditions for thermodynamically distinct phases are illustrated. Only the hypoeutectoid part of the equilibrium diagram, where 0.02 wt.% < C% < 0.76 wt.%, is studied in this paper. Regarding this part, there are two features which are critical: first, the starting temperature A_{e1} at which the eutectoid reaction occurs; second, the finishing temperature A_{e3} at which the ferrite (α) can fully transform to austenite (γ). The A_{e1} is normally a single temperature above 973 K; whereas the A_{e3} is about 1183 K for pure iron and progressively decreases by the addition of carbon. As summarized by Garcia de Andrés et al. (2002) and Surm et al. (2004), this is because the solubility of carbon in ferrite (α) is low and ferrite alone can only begin to transform to austenite (γ) at high temperatures, but if cementite decomposes and yields its carbon to the transformation front, the reaction from ferrite to austenite can proceed at lower temperatures.

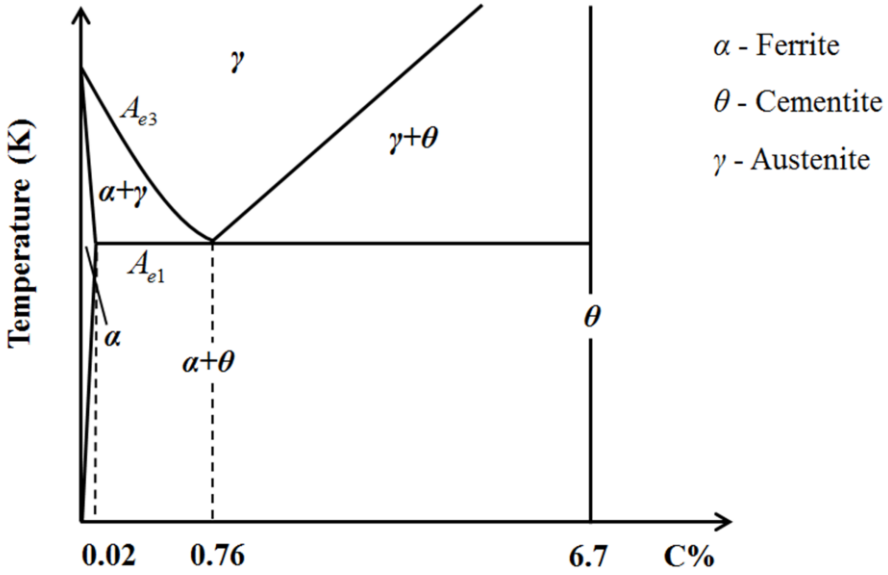

(a) Fe-C equilibrium phase diagram

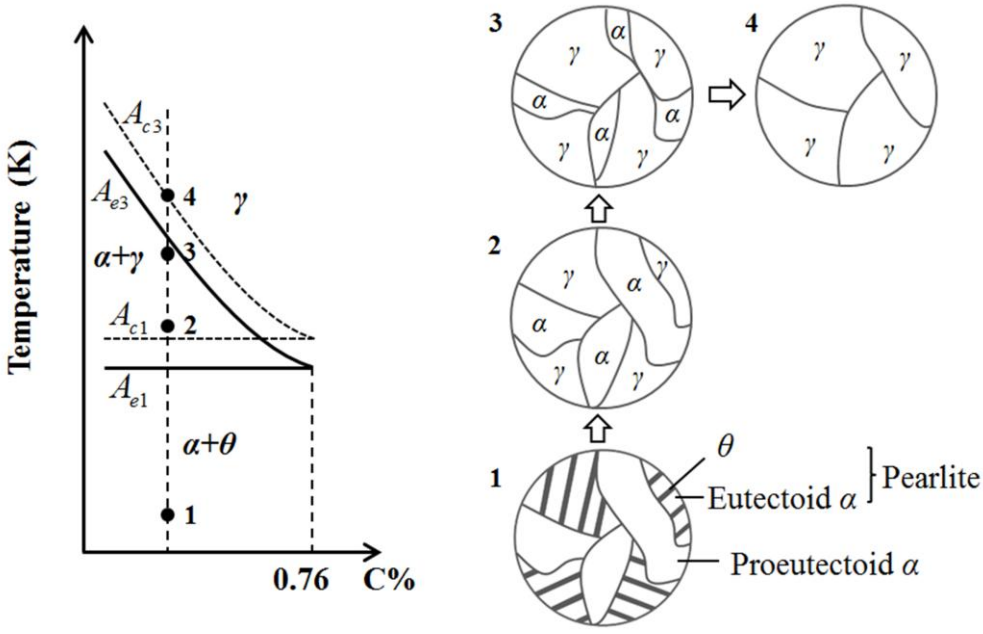

(b) The phase transformation process

Figure 1 Austenite formation in a hypoeutectoid steel (containing less than 0.76 wt.% C)

(a) Fe-C equilibrium phase diagram (b) Phase diagram of hypoeutectoid steel and the schematic representations of the microstructure evolution.

However, the preheating of steel is continuous for most practical hot forming applications. The formation of austenite in a hypoeutectoid steel generally involves heating an aggregate of ferrite + cementite ($\alpha + \theta$) through the two phase ($\alpha + \gamma$) region into a single austenite (γ) phase. In this condition, according to William D. Callister (2005), the beginning and end of the transformation are shifted to higher temperatures A_{c1} and A_{c3}, which are sensitive to the heating rate. Therefore, as schematically shown in Figure 1(b), the phase diagram is modified, in dotted lines, for transformations that occur in continuously increasing temperature conditions. The formation of austenite in a hypoeutectoid steel during continuous heating is schematically illustrated in the figure as well. As can be seen in Figure 1(b-1), the initial microstructure of a hypoeutectoid steel is composed of pro-eutectoid ferrite (α) and pearlite, the latter being a composite of eutectoid ferrite (α) and cementite (θ). The phase composition of the mixture is determined by the amount of carbon in the steel. With an increase in atom mobility and driving force during heating, the pearlite regions firstly become unstable above temperature A_{c1}. For real microstructure, a pearlite region contains numbers of colonies in which lamellae of ferrite and cementite with various sized spacing and orientations are located. Caballero et al. (2000) reported that austenite nucleation primarily takes place at the intersections or interfaces of pearlite colonies, and also at the interfaces of ferrite-cementite lamellae within a colony The new grains of austenite grow into pearlite colonies to replace the eutectoid ferrite; at the same time, the cementite dissolves in the austenite. Once the pearlite is consumed (Figure 1(b-2)), the reaction proceeds into the remaining pro-eutectoid ferrite. Below the finishing temperature, the ferrite can only transform to austenite with additional carbon provided. Carbon atoms diffuse from inside the enriched austenite grains to γ/α interfaces and cross them, which enables the transformation from pro-eutectoid ferrite to austenite. The γ/α interfaces gradually move towards α phase regions (Figure 1(b-3)). This

process continues until temperature A_{c3} is reached, when the average carbon content in austenite becomes equal to the carbon content of the steel. The steel is then fully austenitic (Figure 1(b-4)). If the steel is annealed in the intercritical ($\alpha + \gamma$) region, full austenite formation cannot be achieved. According to (G. R. Speich, 1981), given sufficient soaking time, the volume fraction of austenite at final equilibration is a function of the intercritical annealing temperature. It is noted that, in this study, the kinetics of austenitization is assumed to be mainly a carbon diffusion-controlled process. This is because the diffusivity of carbon in steel is nearly $10^5 – 10^6$ times greater than that of substitutional solutes (e.g. Mn), as reported by Khaira et al. (1993). Therefore, for hot stamping of boron steels in industrial applications, within the practical soaking time, the establishment of equilibrium is with respect to carbon without taking substitution solutes into account.

3. Modelling of austenite formation in selective heating and hot stamping

3.1 Extended volume fraction of austenite

At the first step of the modelling, the equations involve calculation of the extended volume fraction of the growing austenite phase. The definition of extended volume is based on a hypothesis assuming that nucleation and growth apply to an infinite volume of untransformed material, where every single nucleus is unaffected by the formation and growth of other nuclei, as stated by Liu et al. (2007) and Chen et al. (2010). In this study, the extended volume fraction of austenite represents the extended volume of transformed austenite phase in a unit of real sample volume and is represented by f'_A. Under this situation, the development of equations for nucleation and growth of austenite is described below.

According to classic theory, as mentioned by Gaude-Fugarolas and Bhadeshia (2003), nucleation rate is defined as the number of nuclei (particles of supercritical size) formed per unit volume, per unit time. It is determined by the number of particles of critical size and the rate of the jumping of atoms through the interface between the initial phase and the particles of critical size. From the research by Liu et al. (2007), for significant overheating conditions, the nucleation rate of austenite can be formulated using an Arrhenius law:

$$\dot{N} = N_0 \exp\left(-\frac{Q_N}{RT}\right) \tag{1}$$

where R is the gas constant, T is the absolute temperature, Q_N is the activation energy for the jumping of atoms through the interface, and N_0 is the pre-exponential factor. This equation describes a nucleation mode that is constant rate at a constant temperature without pre-existing nuclei (i.e. when t = 0, the number of nuclei: N = 0). Both Q_N and N_0 are temperature- and time- independent.

The pre-exponential factor N_0 can be formulated by characterizing the effects of influencing factors on the austenite formation. The internal influencing factors are related to the starting microstructure of the material, and the external ones are related to heating rate and temperature. For austenite nucleation in pearlite, Roósz et al. (1983) have investigated its dependence on material structure. N_0 was proposed as a morphological function of interlamellar spacing (λ), the edge length of the pearlite colony (α^p), and the number of nucleation sites (N_C):

$$N_0 = f(\lambda, a^p, N_C) \tag{2}$$

Furthermore, Caballero et al. (2000) extended the applications to non-isothermal conditions by adding the effects of heating rate ($\dot{T}$):

$$N_0 = f(\lambda, a^p, N_C, \dot{T}) \tag{3}$$

In this study, because the model is specialized for a particular steel, the morphological parameters in equations (2) and (3) can be simply merged. It was found in (Li et al., 2016) that, during heating, the temperature and time to attain a particular amount of austenite increase and decrease with increasing heating rate, respectively, according to a power law. Hence, the nucleation rate can be modelled by:

$$\begin{aligned} \dot{N} &= \left(A_0 + A_1 \dot{T}^{\varphi_A}\right) \exp\left(-\frac{Q_N}{RT}\right) && (f_A \le f_P) \\ &= 0 && (f_A > f_P) \end{aligned} \tag{4}$$

where Q_N is associated with the activation energy for nucleation, R is the gas constant, $\dot{T}$ is heating rate; A_0, A_1, and φ_A are constants characterizing the overall effects of internal and external influencing factors; f_A is the transformed volume fraction of austenite, and f_P is the initial volume fraction of pearlite. According to Brooks (1992), austenite formation occurs via two routes: transformation from pearlite to austenite and from pro-eutectoid ferrite to austenite in hypoeutectoid steels. As reported by Savran (2009), when the heating speed is low (e.g. 0.05 °C/s), it is possible that nucleation of austenite grains in pearlite and in pro-eutectoid ferrite both occur in a hypoeutectoid steel, while the transformation proceeds at a much higher rate in the pearlite phase. However, at higher heating rates (e.g. 20 °C/s) only nucleation in pearlite is observed because there is not enough time for carbon to diffuse to pro-eutectoid ferrite to stimulate austenite nucleation there. The heating rates studied here are higher (lower heating rates are not suitable in hot stamping applications because they are inefficient), hence it is assumed that nucleation of austenite occurs only in pearlite colonies at the beginning of the transformation. The influence of this assumption on the accuracy of the modelling work is believed to be negligible. Thus equation (4) defines continuous nucleation

and site saturation modes for the first and second step of the austenite formation, respectively. When dissolution of pearlite has finished ($f_A > f_P$), the saturation of nucleation sites causes a zero nucleation rate for the austenite-ferrite transformation. The first term in equation (4) represents static nucleation of austenite, and the second is related to the dynamic effect of heating on austenite nucleation for $f_A \leq f_P$.

Similar to the nucleation rate, the volume growth rate of a nucleus ($\dot{v}$) is modelled by an Arrhenius law:

$$\dot{v} = v_0 \exp\left(-\frac{Q_v}{RT}\right) \tag{5}$$

where Q_v is the activation energy for the volume growth, and v_0 is the pre-exponential factor. According to (Liu et al., 2007) and (Chen et al., 2010), analytically, Q_v is a function of the activation energy for the front migration (Q_{mig}), the growth mode parameter (m') and the dimensionality of the growth (d)

$$Q_v = f(Q_{mig}, m', d) \tag{6}$$

At the same time, the pre-exponential factor v_0 is given as:

$$v_0 = f(g, \eta) \tag{7}$$

where g is a particle-geometry factor and η is a growth factor determined by solute concentrations of the transformed and initial phases. And (6) and (7) can be formulated in various complex ways, depending on the growth mode (interface controlled growth, volume diffusion controlled growth, or mixed-mode growth).

Considering the trade-off between modelling comprehensiveness and mathematical simplicity, for the particular steel in this study, a straightforward equation to describe the volume growth rate of an austenite particle is proposed as:

$$\dot{v} = \left(B_0 + B_1 \dot{T}^{\varphi_B} \right) \exp\left(-\frac{Q_v}{RT} \right) \tag{8}$$

where Q_v is a material constant associated with the activation energy for volume growth which is independent of temperature and time; and B_0, B_1, and φ_B are material constants to be determined from experimental data. Q_v, B_0, B_1, and φ_B can be piecewise defined if the growth mode changes during transformation.

Assuming that all austenite nuclei grow at the same rate under the same thermal conditions, the growth rate of the extended volume fraction of austenite ($\dot{f}'_A$) can be calculated by:

$$\dot{f}'_A = N\dot{v} \tag{9}$$

Equation (9) expresses that the growth rate of extended volume fraction at any time is determined by both the existing quantity of formed nuclei and the instantaneous growth rate of the nuclei.

3.2 Real volume fraction of austenite

Normally, since there is more than one nucleus growing during transformation, the extended volume of transformed phase should be correlated to real volume by taking impingement into account. The widely used model proposed by Avrami (1941) is presented below:

$$f = 1 - \exp(-f') \tag{10}$$

where f is the real volume fraction of transformed phase. The interpretation of equation (10) can be made based on its differential form: $df/dt = (1-f)\, df'/dt$, which means, for a time increment dt, the extended volume fraction increment of transformed phase is df', but only

part, as large as the untransformed volume fraction $(1-f)$, will contribute to the change in real volume fraction *df*. The differential form can also be expressed as:

$$\dot{f} = (1-f)\dot{f}'$$

(11)

where $\dot{f}$ is the rate of *f* with time, and $\dot{f}'$ is the rate of *f'* with time.

As described by Lenel (1983), towards the end of the reaction when a large amount of austenite has been formed, impingement of neighbouring growth centres (or their diffusion fields) will occur, which slows down the reaction rate and increases the time taken to reach equilibrium. This classical theory accounts for the overlap of growing particles (hard impingement), and equations (10) and (11) are restricted to the case of hard impingement with all nuclei randomly dispersed. With respect to diffusion controlled transformations, as mentioned by (Gaude-Fugarolas and Bhadeshia, 2003), the transformation rate slows down when diffusion fields surrounding the new phase particles start to overlap. This mode is denoted as soft impingement. In order to adapt the theory to complex nucleation and growth modes, appropriate adjustments of the formulation are necessary.

Therefore, for the purpose of correlation, an equation extended from equation (11) to describe the real volume fraction of austenite in this study is proposed as:

$$\dot{f}_A = \left(1-{f_A}^m\right)\frac{\dot{f}'_A}{(1+f'_A)^n} \qquad (12)$$

where f_A is the real volume fraction of austenite, $\dot{f}_A$ is the rate of f_A with time; f'_A is the extended volume fraction of austenite, $\dot{f}'_A$ is the rate f'_A; *m*, which is related to the initial volume fraction of pearlite (f_P), and *n* are transformation related parameters given by:

$$\begin{aligned} m &= 1 && (f_A \le f_P) \\ &= 1 - m_0 (f_A - f_P) && (f_A > f_P) \end{aligned} \tag{13}$$

$$n = n_0 \dot{f}_A^{\varphi_n} \tag{14}$$

where m_0, n_0, and φ_n are constants.

3.3 Saturated volume fraction of austenite

As stated in Section 2, only partial austenite formation can be achieved when the boron steel is annealed at an intercritical (α + γ) temperature. According to previous studies conducted by Li et al. (2016), an apparent saturation limit could be observed after 15min, corresponding to the soaking completion of the carbon diffusion process. As explained earlier, the constrained equilibrium respect to carbon is reasonable for modelling of hot stamping processes within the practical soaking time of industrial applications.

In this study, the volume fraction of austenite based on the constrained equilibrium of carbon diffusion is termed the saturated volume fraction of austenite, f_{As}. According to the experimental investigation detailed in (Li et al., 2016), f_{As} can be represented as a function of temperature T:

$$f_{As} = g(T) \tag{15}$$

Equation (15) is an empirical formula and can be determined through experimental data.

The equations developed in section 3.2 are applied for full austenite formation in the γ region. Adjustments are required to adapt the model for intercritical transformations. It was found from the experimental results that isothermal austenite formation at different intercritical

temperatures followed the same trend approaching equilibration; detailed analysis can be found in (Li et al., 2016). Therefore, it is reasonable to substitute the term $\left(1-f_A^{\ m}\right)$ in equation (12), which indicates 100% austenite formation, with ($f_{As}^{\ m}-f_A^{\ m}$) (partial austenite formation). Then equation (12) becomes:

$$\dot{f}_A=\left(f_{As}^{\ m}-f_A^{\ m}\right)\frac{\dot{f}_A'}{(1+f_A')^n} \tag{16}$$

3.4 The complete constitutive model

By introducing variables such as extended volume, saturated volume fraction, and volume fraction of austenite, a set of coupled constitutive equations, which are based on the mechanisms of nucleation, growth and impingement, can be formulated to model the austenite formation in boron steel subjected to hot stamping.

When $T > A_{c1}$,

$$\begin{aligned}\dot{N}&=A_1\left(A+\dot{T}^{\varphi_A}\right)\exp\left(-\frac{Q_N}{RT}\right) && (f_A\le f_P)\\ &=0 && (f_A> f_P)\end{aligned} \tag{17}$$

$$\dot{v}=B_1\left(B+\dot{T}^{\varphi_B}\right)\exp\left(-\frac{Q_v}{RT}\right) \tag{18}$$

$$\dot{f}_A'=N\dot{v} \tag{19}$$

$$\dot{f}_A=\left(f_{As}^{\ m}-f_A^{\ m}\right)\frac{\dot{f}_A'}{(1+f_A')^n} \tag{20}$$

where

$f_{As}=g(T)$ and the parameters *m* and *n* are defined as:

$$\begin{aligned} m &= 1 && (f_A \le f_P) \\ &= 1 - m_0(f_A - f_P) && (f_A > f_P) \end{aligned} \tag{21}$$

$$n = n_0 \dot{f}_A^{\varphi_n} \tag{22}$$

In this set of equations, A_{c1} is the starting temperature of austenite formation under continuous heating, according to (Li et al., 2016), defined as when f_A = 2% (2% is the value which can be experimentally detected), and it is related to heating rate by a power law:

$$A_{c1} = 1000\dot{T}^{0.0043} \tag{23}$$

$\dot{N}$ and N are the nucleation rate and nuclei of austenite per unit sample volume, respectively; $\dot{v}$ is the volume growth rate of an austenite nucleus; V_e is the extend volume of transformed austenite per unit sample volume, and its growth rate is modelled using equation (19); f_A is the volume fraction of austenite and its formation rate is expressed by equation (20); f_{As} is the saturated volume fraction of austenite as a function of temperature; m and n are parameters to characterise the impingement mechanism; R is the gas constant and T is the absolute temperature; f_p is the volume fraction of pearlite in the initial structure; A_1, A, φ_A, Q_N, B_1, B, φ_B, Q_v, m_0, n_0, φ_n are constants to be determined from experimental data.

The complete constitutive model is used in this study for the development of the austenite formation model consisting of multiple evolutionary equations. The variables in equations (17) – (22) have their individual physical meanings related to the microstructural evolution during austenite formation processes. The features and interactive effects of physical phenomena during the transformation can thus be described. It is noted that the morphological parameters of the material are merged and not counted individually in the equations, which allows the simplicity of modelling work.

The materials model, equations (17) – (22), is a set of Ordinary Differential Equations (ODE) in terms of time *t*, which can be solved with given initial values for the variables. Thus this is also known as the solution for an initial value problem. In the numerical integration of solving the equations, at $t = 0$, N, v, and f'_A are equal to 0; f_A is equal to 2% and starts to integrate only when temperature is above $A_{c1.}$ Below A_{c1}, austenite formation is not possible.

4. Calibration of the constitutive model

4.1 Experimental programme and results

The material used in this study was a 22MnB5 manganese-boron steel from ThyssenKrupp Steel, provided by the project sponsor SAIC MOTOR. It was cold rolled and hot-dip aluminized. The initial microstructure contained an approximate 78%/22% mixture of proeutectoid ferrite and pearlite; the chemical composition of the steel is listed in Table 1.

Table 1 Chemical composition (Max value - ladle analysis in wt.%)

C	Si	Mn	P	S	Cr + Mo	Ti	*B*
0.25	0.40	1.40	0.025	0.010	0.50	0.05	0.005

The austenite formation involves a lattice change of iron from a body-centred cubic (BCC) form to a face-centred cubic (FCC) form, which results in a change in density, hence volume. Therefore the evolution of the transformation can be deduced from experimental dilatometry, which was presented in the studies by Reed et al. (1998). Experiments were carried out using a Gleeble 3800 thermo-mechanical testing system. Rectangular specimens cut from the same

piece of 1.6 mm thickness sheet were used for the tests. The initial gauge length of the specimen was 20 mm and the width was 10 mm.

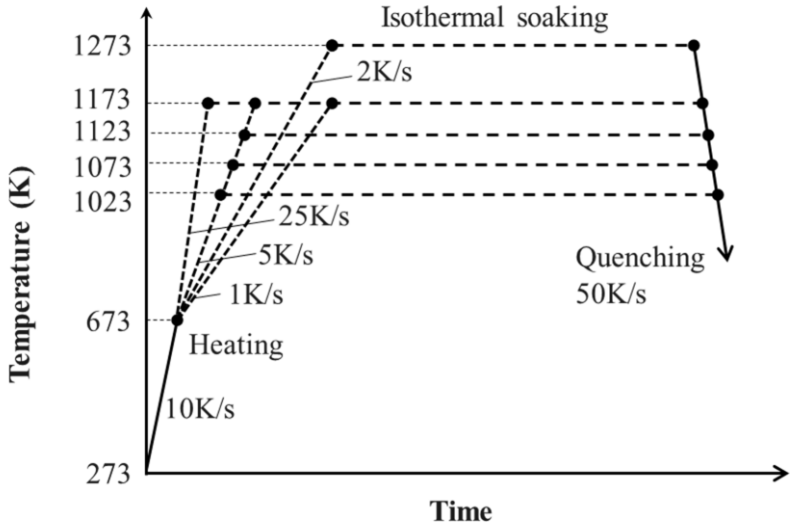

Figure 2 Test programme with different heating rates and soaking temperatures.

Figure 2 shows the heat treatment test programme, which was designed to match the thermal cycle used in practice for the hot stamping of boron steel, consisting of continuous heating, isothermal soaking and quenching. In order to characterize the effects of heating rate and temperature on the austenite formation, two groups of tests were designed: in the first group, specimens were heated to 1173 K at different heating rates from 673 K. 1173 K is the soaking temperature adopted for full austenitization in hot stamping practice for this boron steel, as established by Li et al. (2014). Long soaking periods were applied to enable a saturated volume fraction of austenite to be obtained: 10 min for 1 K/s and 15 min for 5 K/s and 25 K/s. In the second group, specimens were heated at the same heating rate of 5 K/s to different temperatures of 1023 K, 1073 K, 1123 K and 1173 K, and soaked for 15 min. In addition, in order to validate results predicted by the model, a third testing programme was designed: a

specimen was heated to 1273 K at a heating rate of 2 K/s, and soaked for 2 min without reaching saturation of austenite. After isothermal soaking, all specimens were quenched at a cooling rate of 50 K/s, which ensured complete transformation from austenite to martensite, per the results of Li et al. (2012).

To quantitatively relate the results of dilatometry to the extent of austenite formation, a method was developed to calculate the volume fraction of austenite from dilatometric data; details can be found in (Li et al., 2016). The evolution of austenite volume fraction with temperature and time are presented in Figures 3 and 4 (symbols). In the figures, time t = 0 corresponds to temperature T = 873K, instead of room temperature, to reduce unnecessary data points (this also applies to the figures that follow). As shown in Figure 3 (a) regarding the first group of tests, the transformations progress differently during continuous heating for different heating rates. The starting temperature A_{c1} (defined as when f_A = 2% in this study) increases with increasing heating rate: for the heating rate of 1 K/s, A_{c1} = 1000 K; for 5 K/s, A_{c1} = 1007 K; and for 25 K/s, A_{c1} = 1114K. When the continuous heating ends at 1173 K, the amount of transformed austenite decreases with increasing heating rate: for 1 K/s, the volume fractions of austenite are f_A = 77%; for 5 K/s, f_A = 61%; and for 25 K/s, f_A = 54%. This is mainly because a higher heating rate means less soaking time is available for diffusional transformation with a given growth geometry, which is consistent with results presented by Huang et al. (2004) and Cai (2011). Subsequently, the volume fractions of austenite keep increasing until about 100% at different rates despite the soaking temperature being the same: at the same stage of the transformation (e.g. f_A = 80%), according to the slope of the curves in Figure 3 (a-right), the volume fraction of austenite exhibits a higher increasing rate for the pre-heating rate of 25 K/s, than for 5 K/s and 1 K/s. As shown in Figure 3 (b) regarding the second group of tests, with increasing soaking time the volume

fractions of austenite increase and then become almost constant at particular values less than 100%, which are taken to be the saturated volume fractions of austenite (f_{As}) corresponding to the soaking temperatures: for 1023 K, the saturated volume fraction of austenite f_{As} = 32%; for 1073 K, f_{As} = 83%; for 1123 K, f_{As} = 92%; and for 1173 K, f_{As} = 99%. As shown in Figure 4 regarding the third group of tests, the austenite volume fraction reaches 81% when continuous heating ends, and then increases to 89% after 2 min of soaking at 1273 K.

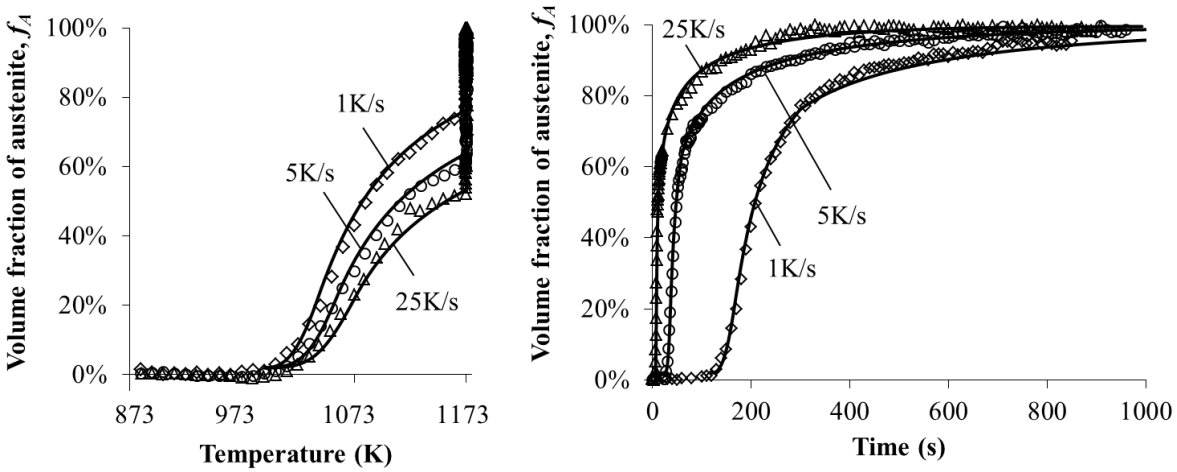

(a) Different heating rates (soaking temperature: 1173 K)

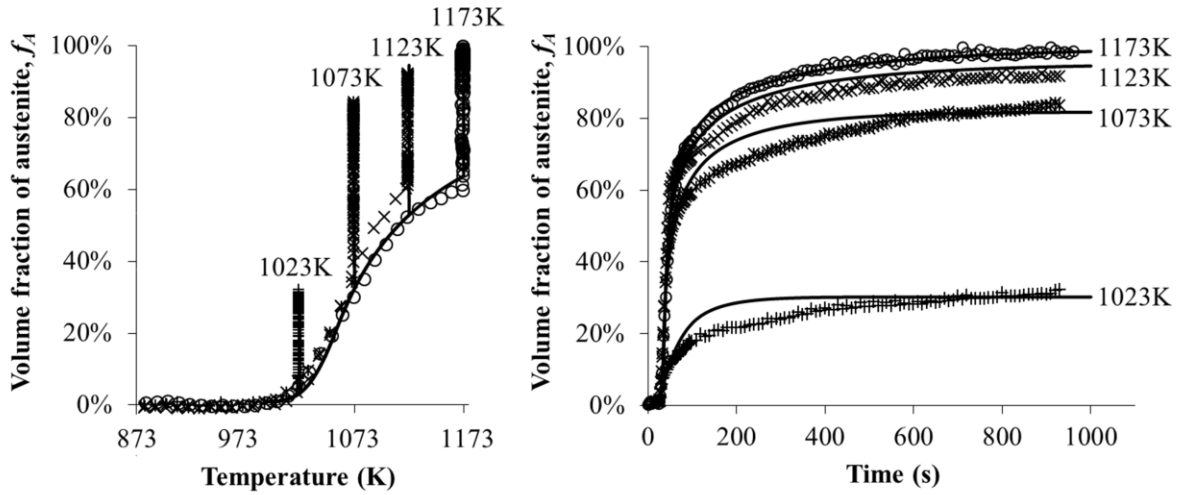

(b) Different soaking temperatures (heating rate: 5 K/s)

Figure 3 Comparison of experimental (symbols) and computed (solid curves) volume fractions of austenite formation under different heating conditions for calibration.

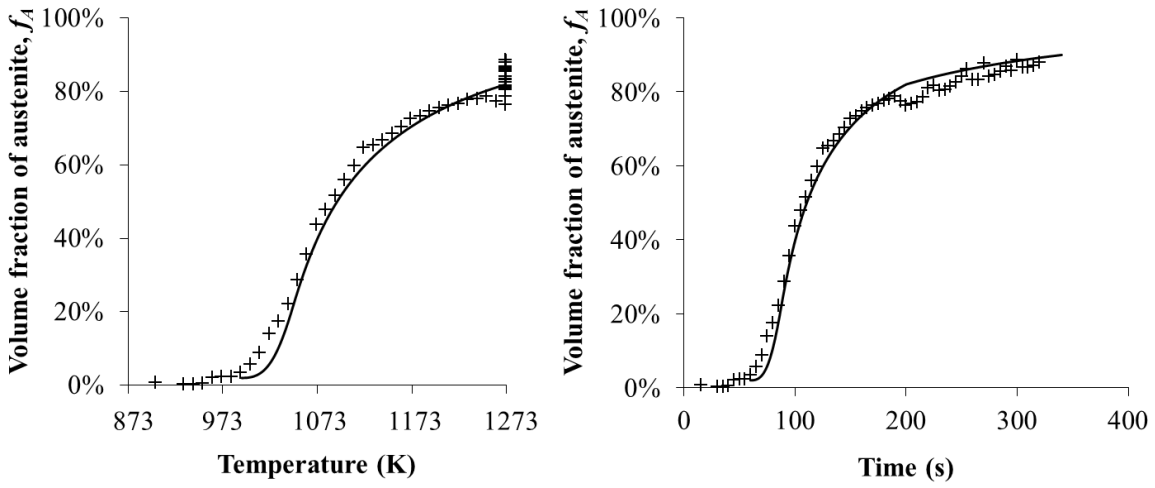

Figure 4 Comparison of experimental (symbols) and predicted (solid curves) volume fractions of austenite formation for validation (Heating rate: 2 K/s and soaking temperature: 1273 K).

4.2 Calibration of the constants from experimental data

The model was calibrated by fitting the computed volume fraction of austenite to the experimental results by adjusting the values of the constants within the equations. A trial-and-error method was adopted in this study, with error quantified in a least squares sense.

The first step of calibration was to determine the saturated austenite volume fraction f_{As} as a function of temperature. As shown in Figure 5, an empirical formula was determined as:

$$f_{As} = \min \begin{cases} \dfrac{C_2}{\pi} \arctan\left(C_1 \left(\dfrac{T}{T_{As}} - 1 \right) \right) + C_3 \\ 1 \end{cases} \tag{24}$$

The values of the constants in the equation were adjusted to get the best fit to the experimental points at 1023 K, 1073 K, 1123 K, and 1173 K, as shown by the symbols in Figure 5. The calibrated constants are listed in Table 2.

Table 2 Calibrated constants for equation (24), determined from the experimental data.

C_1	C_2	C_3	T_{As} (K)
36.0	1.2	0.475	1037

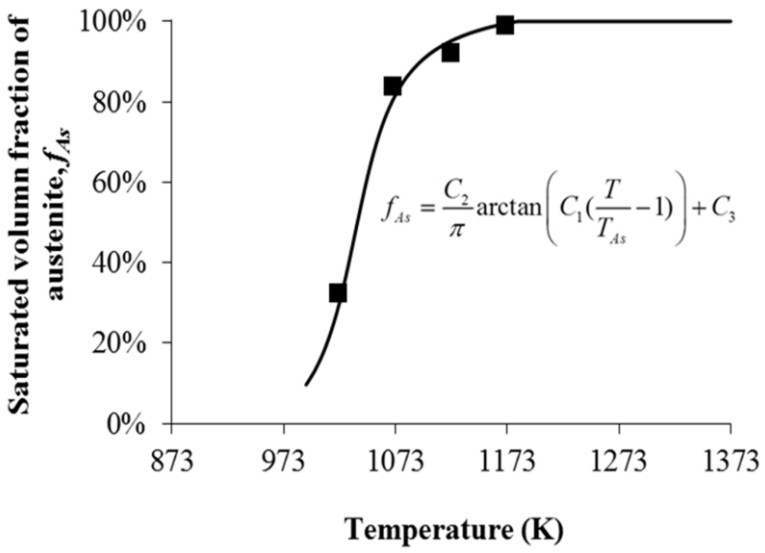

Figure 5 Comparison of experimental (symbols) and computed (solid curve) saturated volume fraction of austenite at intercritical annealing temperatures using equation (21).

At the second step, the computation was conducted in an iterative and incremental manner. Equations (17) – (22) were numerically integrated using the forward Euler method. The input was the initial values of the state variables and temperature profile. The temperature to start

the integration is A_{c1} which is related to heating rate and given by the empirical equation (23), with the initial value of f_A of 2% (as explained earlier); at the same time, the initial values of N, v, and f'_A were defined as zero, and f_{As} was given by employing equation (24). The output was the integrated values of the variables. The evolution of f_A was used for fitting with the experimental curves. Figure 3 shows the comparison of experimental (symbols) and computed (solid curves) volume fraction of austenite formation with temperature and time under different heating rates and soaking temperatures. Good agreement has been obtained and the features of the experimental data are exhibited clearly by the computed curves. The calibrated constants are listed in Table 3. It is noted that, equations (17) – (22) were mechanism-based formulations and the constants in the equations are associated with physical meanings; on the other hand, since the morphological parameters of the material are merged for the purpose of simplicity for industrial applications, the constants don't need to represent the real values of individual physical parameters, e.g. the product of A_1 and B_1 need not be decoupled. In this case, the set of constants in this study fits only this particular steel variant. Empirical formulae (23) and (24) and the constants in Table 2 and Table 3 will be re-determined when the initial microstructure of the steel is changed.

Table 3 Calibrated constants for equations (17) – (22), determined from the experimental data.

Q_N (J/mol)	Q_v (J/mol)	$A_1 \cdot B_1$	A	B	φ_A
1.486e5	4.05e4	2.394e6	0.8	1.0	1.41
φ_B	m_0	f_P	n_0	φ_n	R (J/mol·K)
0.12	1.05	0.22	2.1	0.155	8.314

4.3 Validation and analysis

To validate the calibrated material model, a further computation was carried out using the determined material constants listed in Table 2 for a heating rate of 2 K/s, and soaking at 1273 K for 2 min. As shown in Figure 4, the predicted volume faction of austenite with temperature and time (solid curves) both agree well with the experimental data (symbols). Prediction of the continuous heating transformation (CHT) diagram is very valuable for guiding the design of heat treatment in practice. In Figure 6, the temperature and time required to attain the chosen volume fractions of austenite (10%–70%) under continuous heating at different heating rates (1–25 K/s) were predicted using the calibrated model. The computed CHT data is represented by solid curves. The data points that are available from the experimental results are indicated by cross symbols in the figure. Most of the symbols lie on or close to the computed curves, which again shows the reliability of the model.

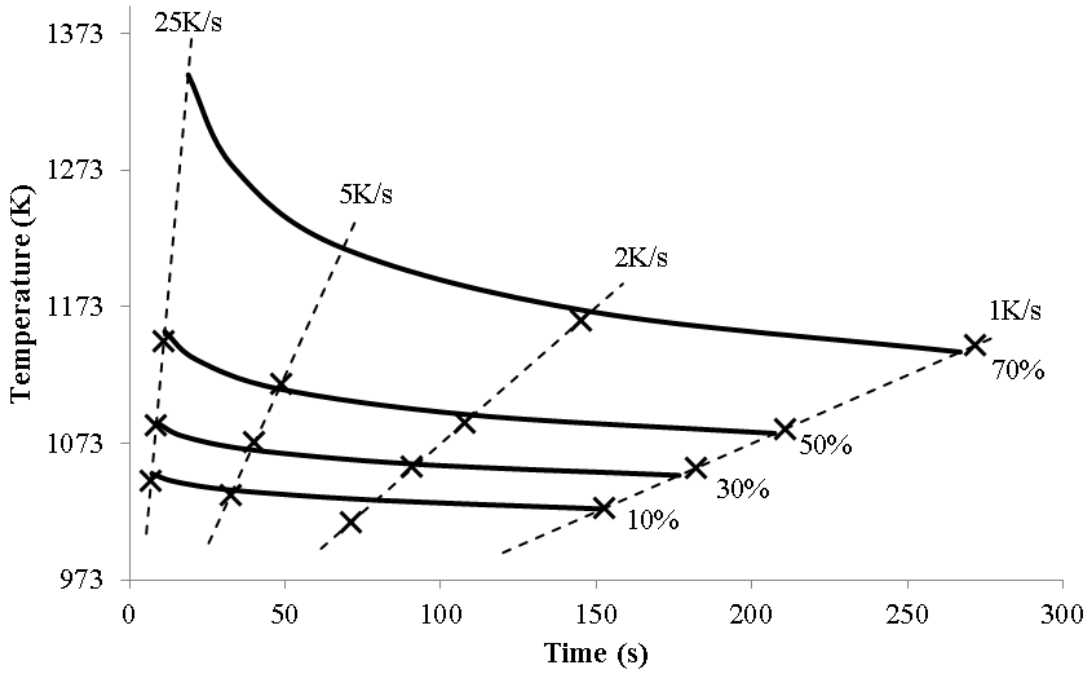

Figure 6 Comparison of experimental (symbols) and predicted (solid curves) continuous heating transformation (CHT) data, which are shown for different volume fractions of austenite (10%–70%) with various heating rates (1–25 K/s).

Control of the soaking time is of great importance in enhancing productivity and reducing cost in practice. In Figure 7, the soaking time increments $\Delta t_{80\%\text{-}90\%}$ (the time elapsed for austenite formation from f_A = 80% to f_A = 90%) at 1173 K with different pre-heating rates (1–25 K/s) have been predicted. The relationship between heating rate and soaking time increment was summarised as a solid line on a log-log scale. The symbols are the experimental data. Good agreement is shown again in this case. The predicted trend indicates that for a chosen stage of transformation and a chosen soaking temperature, less time is required for the steel preheated at a higher rate. This is consistent with the discussion on experimental results earlier and provides guidance for optimising the thermal conditions of hot stamping processes.

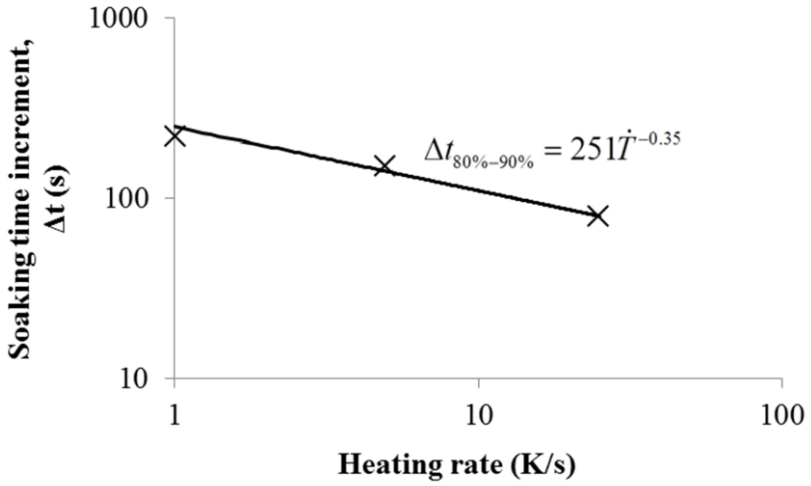

Figure 7 Comparison of experimental (symbols) and predicted (solid line) relationships of time increment to attain 80%–90% austenite volume fraction under an isothermal condition (1173 K) with heating rate.

5. Conclusions

A set of coupled constitutive equations has been developed to describe the austenite formation in a manganese boron steel for hot stamping heating processes, determined and calibrated from experimental data. The model is physically-based and has potential for application to other steels. In addition, the model has the following features:

- The austenite formation under both non-isothermal and isothermal conditions can be described; the effects of heating rate have been taken into account for the subsequent isothermal transformation.
- Both full and partial austenite formation at γ and $(\alpha + \gamma)$ regions is captured.
- The state variables expressed in terms of evolution rate enable the model to be solved easily through numerical integration.
- The calibrated model gives accurate predictions of the austenite formation progress, which has been validated by experimental data. It is meaningful for industrial hot stamping practice.

Acknowledgements

The authors thank SAIC MOTOT UK Technical Centre for financial support and the supply of material.

References

Asadi Asadabad, M., Goodarzi, M., Kheirandish, S., 2008. Kinetics of austenite formation in dual phase steels. ISIJ International 48, 1251–1255.

Avrami, M., 1941. Kinetics of Phase Change. III. Granulation, Phase Change, and Microstructure. Journal of Chemical Physics 9, 177–184.

Azizi-Alizamini, H., 2010. Austenite formation and grain refinement in C-Mn steels, The Faculty of Graduate Studies (Materials Engineering). THE UNIVERSITY OF BRITISH COLUMBIA.

Brooks, C.R., 1992. Principles of the Austenitization of Steels. Elsevier Science Publishers Ltd, London.

Caballero, F.G., Capdevila, C., Garcı´a de Andre´s, C., 2000. Influence of scale parameters of pearlite on the kinetics of anisothermal pearlite to austenite transformation in a eutectoid steel. Scripta mater. 42, 1159–1165.

Cai, J., 2011. Modelling of phase transformation in hot stamping of boron steel, Mechanical Engineering. Imperial College London.

Chen, H., Liu, Y.C., Wang, D.J., Yan, Z.S., Fu, J.C., Shi, Q.Z., 2010. A JMAK-like approach for isochronal austenite–ferrite transformation kinetics in Fe–0.055 wt-%N alloy. Materials Science and Technology 26, 572-578.

G. R. Speich, V.A.D., and R. L. Miller, 1981. Formation of austenite during intercritical annealing of dual-phase steels. Metallurgical Transactions A 12A.

Garcia, C.I., Deardo, A.J., 1981. Formation of austenite in 1.5 pct Mn steels Metallurgical Transactions A 12A, 521-530.

Garcia de Andrés, C., Caballero, F.G., Capdevila, C., Álvarez, L.F., 2002. Application of dilatometric analysis to the study of solid–solid phase transformations in steels. Materials Characterization 48, 101-111.

Gaude-Fugarolas, D., Bhadeshia, H.K.D.H., 2003. A model for austenitisation of hypoeutectoid steels. Journal of Materials Science 38, 1195 – 1201.

Haddad-Sabzevar, M., Haerian, A., Seied-Hossein-Zadeh, H., 2009. A stochastic model for austenite phase formation during arc welding of a low alloy steel. Journal of Materials Processing Technology 209, 3798-3807.

Huang, J., Poole, W.J., Militzer, M., 2004. Austenite formation during intercritical annealing. Metallurgical and Materials Transactions A 35, 3363-3375.

Karbasian, H., Tekkaya, A.E., 2010. A review on hot stamping. Journal of Materials Processing Technology 210, 2103-2118.

Khaira, H.K., Jena, A.K., Chaturved, M.C., 1993. Effects of heat treatment cycle on equilibrium between ferrite and austenite during intercritical annealing. Materials Science and Engineering A 161, 267-271.

Law, N.C., Edmonds, D.V., 1980. The formation of austenite in a low-alloy steel. Metallurgical Transactions A 11-A, 33-46.
Lenel, U.R., 1983. TTT curves for the formation of austenite. Scripta Metallurgica 17, 471-474.
Li, N., Li, X., Dry, D., Dean, T.A., Lin, J., Balint, D., 2012. Investigation on the mechanical properties of as-formed boron steels for optimizing process strategies in hot stamping, The 14th International Conference of Metal Forming 2012, pp. 1259-1262.
Li, N., Lin, J., Balint, D.S., Dean, T.A., 2016. Experimental characterisation of the effects of thermal conditions on austenite formation for hot stamping of boron steel. Journal of Materials Processing Technology 231, 254-264.
Li, N., Lin, J., Dean, T.A., Dry, D., Balint, D.S., 2014. Concept Validation for Selective Heating and Press Hardening of Automotive Safety Components with Tailored Properties Key Engineering Materials 622-623, 1124-1131.
Liu, F., Sommer, F., Bos, C., Mittemeijer, E.J., 2007. Analysis of solid state phase transformation kinetics: models and recipes. International Materials Reviews 52, 193-212.
Oliveira, F.L.G., Andrade, M.S., Cota, A.B., 2007. Kinetics of austenite formation during continuous heating in a low carbon steel. Materials Characterization 58, 256-261.
Parris, D.C., McLellan, R.B., 1976. The diffusivity of carbon in austenite. Acta Metallurgica 24, 523-528.
Reed, R.C., Akbay, T., Shen, Z., Robinson, J.M., Root, J.H., 1998. Determination of reaustenitisation kinetics in a Fe–0.4C steel using dilatometry and neutron diffraction. Materials Science and Engineering A 256, 152-165.
Roósz, A., Gácsi, Z., Fuchs, E.G., 1983. Isothermal formation of austenite in eutectoid plain carbon steel. Acta Metallurgica 31, 509-517.
Savran, V.I., 2009. Austenite formation in C-Mn steel, Materials Science and Technology. the Delft University of Technology.
Schmidt, E.D., Damm, E.B., Sridhar, S., 2007. A study of diffusion- and interface-controlled migration of the austenite/ferrite front during austenitization of a case-hardenable alloy steel. Metallurgical and Materials Transactions A 38A, 698-715.
Surm, H., Kessler, O., Hunkel, M., Hoffmann, F., Mayr, P., 2004. Modelling the ferrite/carbide austenite transformation of hypoeutectoid and hypereutectoid steels. J. Phys. IV France 120, 111-119.
William D. Callister, J., 2005. Fundamentals of Materials Science and Engineering, Second Edition ed. John Wiley & Sons, Inc.

Figure

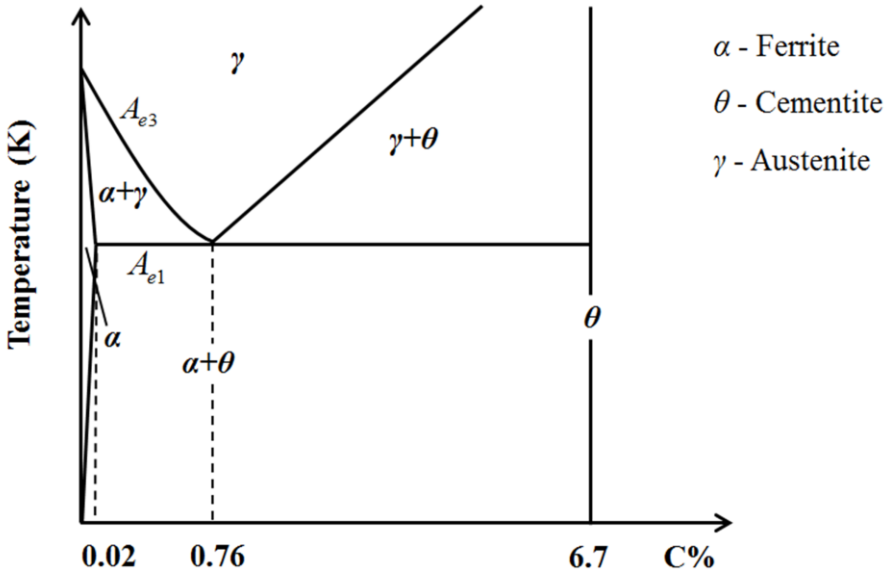

(a) Fe-C equilibrium phase diagram

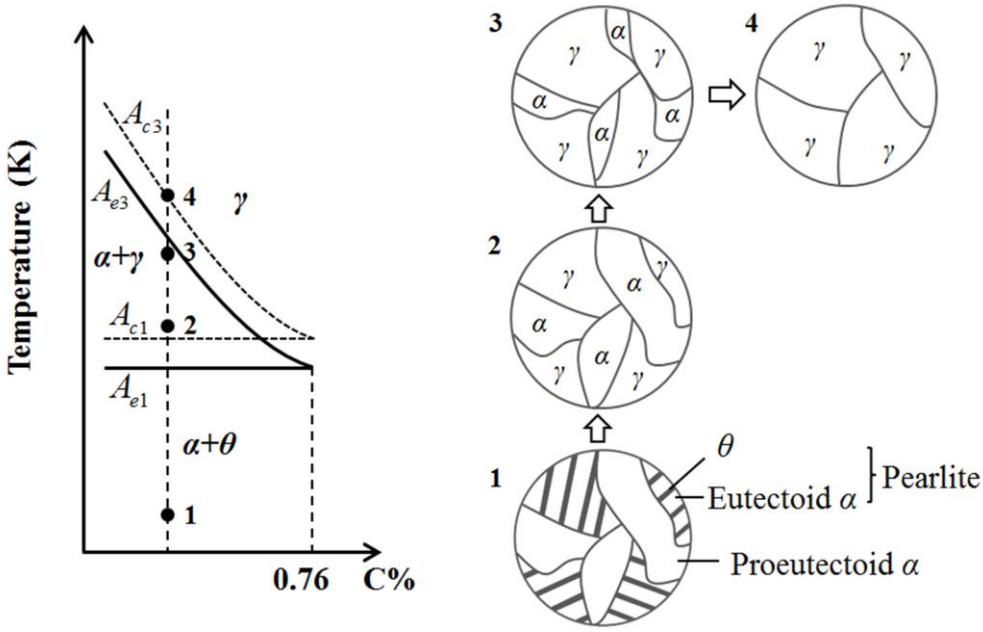

(b) The phase transformation process

Figure 1 Austenite formation in a hypoeutectoid steel (containing less than 0.76 wt.% C) (a) Fe-C equilibrium phase diagram (b) Phase diagram of hypoeutectoid steel and the schematic representations of the microstructure evolution.

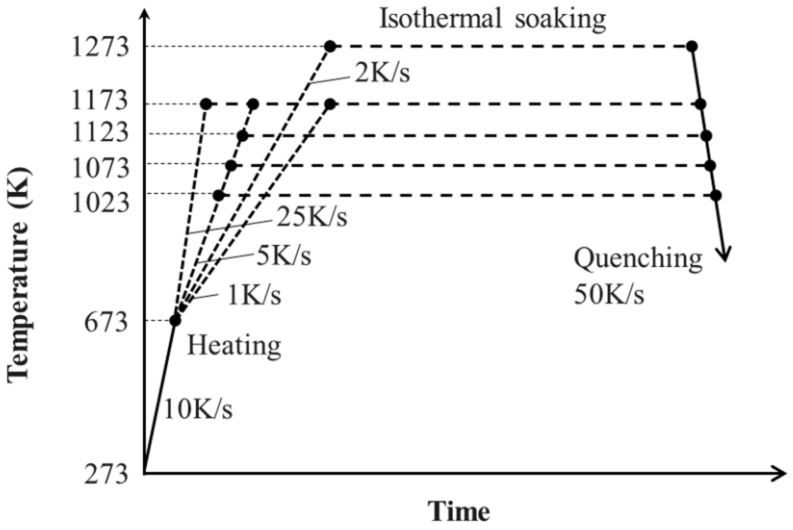

Figure 2 Test programme with different heating rates and soaking temperatures.

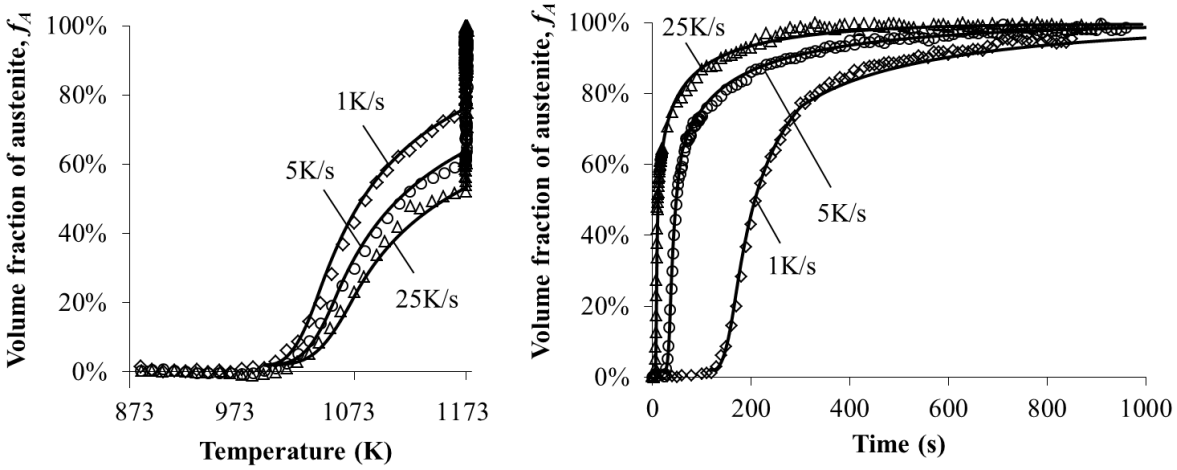

(a) Different heating rates (soaking temperature: 1173 K)

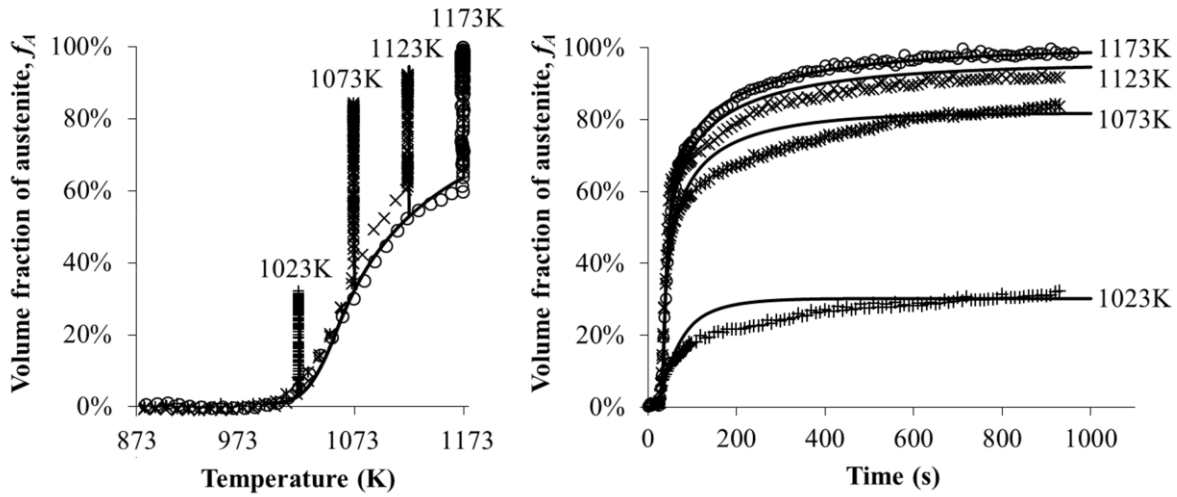

(b) Different soaking temperatures (heating rate: 5 K/s)

Figure 3 Comparison of experimental (symbols) and computed (solid curves) volume fractions of austenite formation under different heating conditions for calibration.

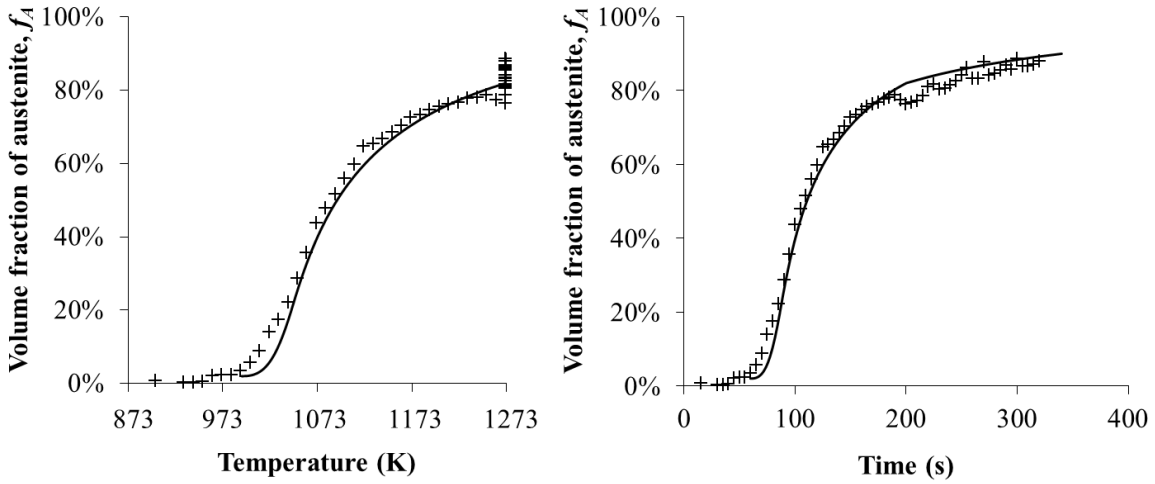

Figure 4 Comparison of experimental (symbols) and predicted (solid curves) volume fractions of austenite formation for validation (Heating rate: 2 K/s and soaking temperature: 1273 K).

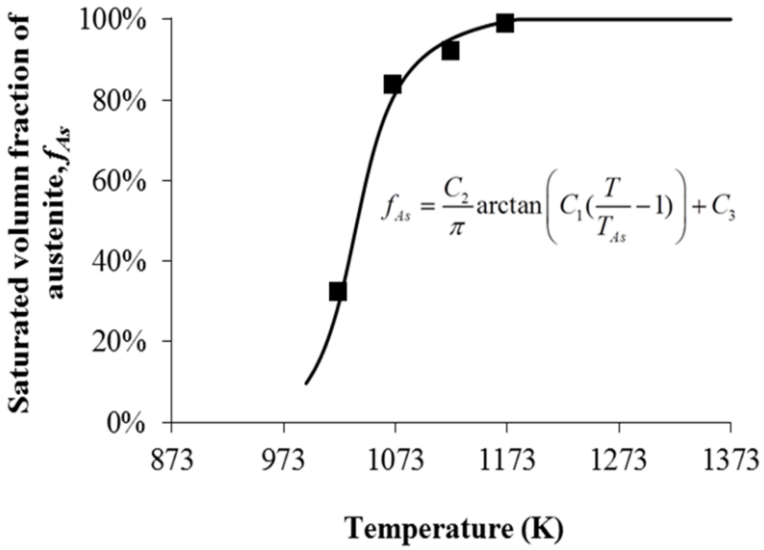

Figure 5 Comparison of experimental (symbols) and computed (solid curve) saturated volume fraction of austenite at intercritical annealing temperatures using equation (21).

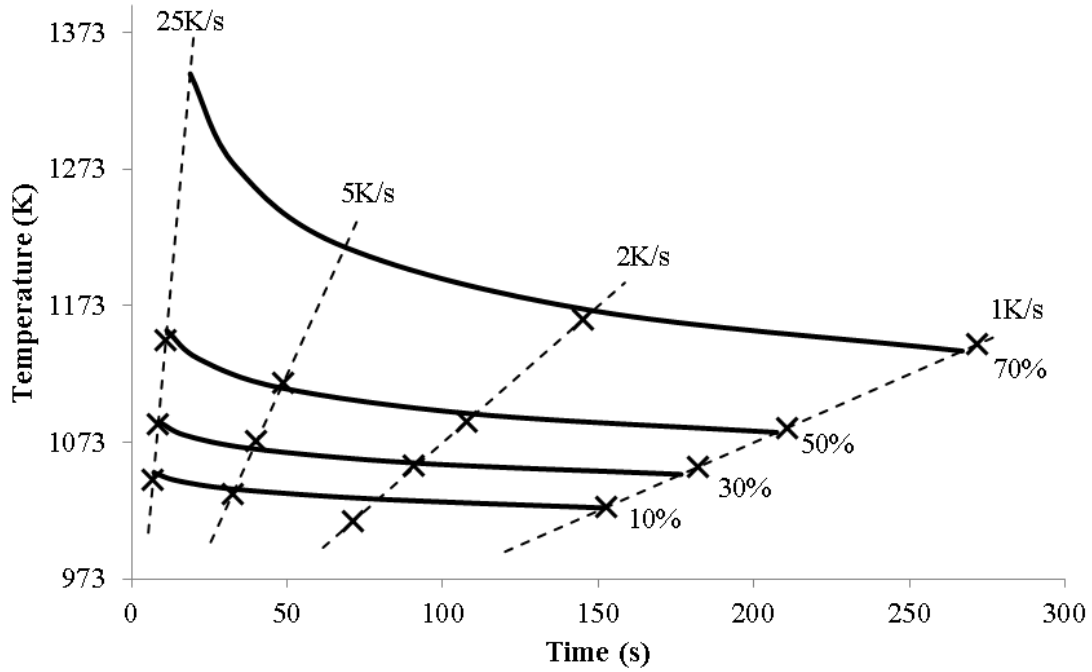

Figure 6 Comparison of experimental (symbols) and predicted (solid curves) continuous heating transformation (CHT) data, which are shown for different volume fractions of austenite (10%–70%) with various heating rates (1–25 K/s).

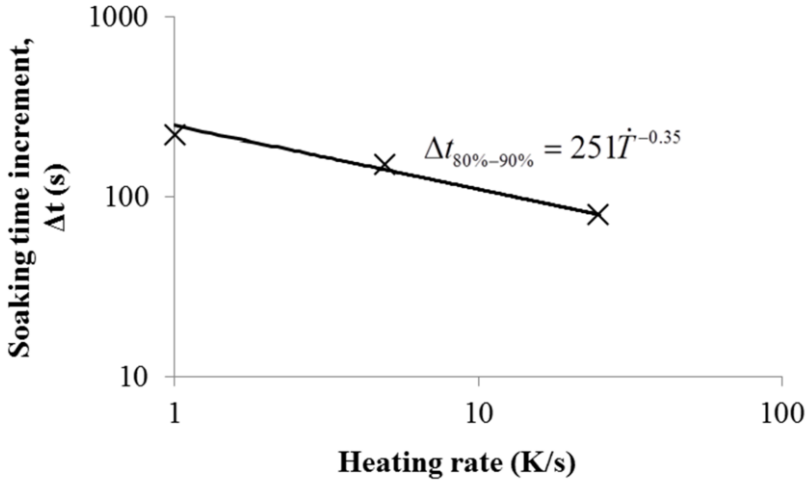

Figure 7 Comparison of experimental (symbols) and predicted (solid line) relationships of time increment to attain 80%–90% austenite volume fraction under an isothermal condition (1173 K) with heating rate.

Table

Table 1 Chemical composition (Max value - ladle analysis in wt.%)

C	Si	Mn	P	S	Cr + Mo	Ti	*B*
0.25	0.40	1.40	0.025	0.010	0.50	0.05	0.005

Table 2 Calibrated constants for equation (24), determined from the experimental data.

C_1	C_2	C_3	T_{As} (K)
36.0	1.2	0.475	1037

Table 3 Calibrated constants for equations (17) – (22), determined from the experimental data.

Q_N (J/mol)	Q_v (J/mol)	$A_1 \cdot B_1$	A	B	φ_A
1.486e5	4.05e4	2.394e6	0.8	1.0	1.41
φ_B	m_0	f_P	n_0	φ_n	R (J/mol·K)
0.12	1.05	0.22	2.1	0.155	8.314